The Dissociation of Gallium–Hydrogen Pairs in Crystalline Silicon during Illuminated Annealing

Jochen Simon,* Axel Herguth, Leah Kutschera, and Giso Hahn

Hydrogen-rich crystalline Si samples are produced by coating Ga-doped Czochralski-grown silicon wafers with SiN$_x$:H and subsequent rapid thermal anneal. This procedure introduces H$_2$ dimers into the bulk, which enables the formation of gallium–hydrogen pairs (GaH). The change in pair concentration can be determined by change in resistivity, as pair formation consumes holes. During illumination at elevated temperature (180 °C), some of the previously formed GaH pairs dissociate into H and/or H$_2$ within hours. A subsequent anneal step forms the pairs again. If illumination is prolonged to days at 180 °C, a second dissociation phase occurs after which GaH pairs do not form again in the dark. Therefore, probably two processes are ongoing: a reversible (fast) one and an irreversible (slow) dissociation of GaH pairs in crystalline silicon. The fraction of dissociated pairs and rate of dissociation depend on temperature and excess charge carrier concentration. This suggests an electron-driven, thermally activated back reaction into either H dimers or atomic hydrogen. An Arrhenius analysis reveals a possibly injection-dependent activation energy of the reversible dissociation process in the range of 0.64–0.71 eV. Lifetime measurements reveal a drastic increase in effective defect density during the second decrease in pair concentration.

1. Introduction

Hydrogen has a strong impact on defect passivation and lifetime-related degradation phenomena such as light and elevated temperature-induced degradation (LeTID),[1–5] both significantly affecting the performance of silicon solar cells. As the underlying mechanisms of LeTID are still unclear and the direct microscopic impact of hydrogen is not tangible, quantifying the hydrogen concentration in the bulk and correlating it to defect densities is a promising route for further investigations. However, quantification of hydrogen in low concentrations is not straightforward. One way is to take advantage of the

J. Simon, A. Herguth, L. Kutschera, G. Hahn
Department of Physics
University of Konstanz
78457 Konstanz, Germany
E-mail: jochen.simon@uni-konstanz.de

The ORCID identification number(s) for the author(s) of this article can be found under https://doi.org/10.1002/pssr.202200297.

formation of acceptor-hydrogen pairs at elevated temperatures in the dark for indirect quantification as it counteracts doping.[6] However, as this method only detects changes in acceptor-hydrogen pair concentration, it is blind for pairs already present in the sample. To capture these as well, it is beneficial if these pairs can be fully dissociated before or after complete formation.

Although the pairing mechanism of hydrogen with acceptors in crystalline silicon has been investigated since the 80s,[6–10] the pairing mechanism of boron–hydrogen pairs recently drew attention in the context of hydrogen determination in crystalline silicon solar cells by either diffusivity analysis,[11] resistivity measurement techniques,[12–17] or spectroscopic approaches.[18,19]

It is known that boron–hydrogen (BH) pairs form from dimers H$_{2A}$, which are present after quenching[20,21] during annealing in the dark in the temperature range up to 300 °C[15,17] whereas they become unstable under illumination/injection and dissociate[13] according to the reaction

$$2B^- + 2h^+ + H_{2A} \underset{\text{formation}}{\overset{\text{dissociation}}{\rightleftarrows}} 2BH^0 \qquad (1)$$
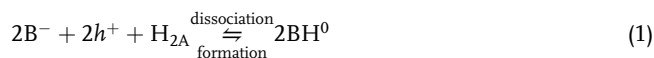
with reaction equilibrium and thus net direction of dynamics depending on initial state, temperature and injection. Hence, applying appropriate illumination conditions allows for a quantification of initially already present and during dark annealing additionally formed BH pairs.

However, with solar cell production predominantly having switched from B-doped to Ga-doped silicon in the last years, the question arises whether gallium–hydrogen (GaH) pairs behave similarly or how conditions, meaning temperature and injection, have to be adapted. Adopted from the case of boron,[11] the predominant reaction of gallium and hydrogen in the dark up to at least 200 °C[16] is

$$2Ga^- + 2h^+ + H_{2A} \rightarrow 2GaH^0 \qquad (2)$$

with holes h^+ being consumed during the splitting reaction H$_{2A}$ + 2h^+ → 2H$^+$ resulting in a change of hole density Δp; thus, $\Delta[\text{GaH}] = -\Delta p$. Whether, or to what degree, this reaction reverses under illumination/injection is not well understood.

Within this article the interplay of GaH pair formation in the dark and dissociation under illumination at elevated temperatures is investigated. The dissociation of the GaH pairs is

ADVANCED SCIENCE NEWS
www.advancedsciencenews.com

pss rrl
physica status solidi
www.pss-rapid.com

particularly important in experiments aiming for the quantification of total hydrogen content via the resistivity method.[12,14]

2. Results

Ga-doped Czochralski-grown Si samples exposed to dark anneal show an increase in resistivity which translates to a decrease in hole concentration p, as shown in **Figure 1**a. The general behavior of the decrease in hole concentration is well described by an exponential rise–saturation curve, assuming first-order dynamics with effective reaction rate R_{form}, change A_{form}, and long-term value A_∞ according to

$$-\Delta p(t) = -A_{form} \times \exp(-R_{form} \times t) + A_\infty \qquad (3)$$

The amount of GaH pairs does not change even for treatment times beyond 10^4 s. In fact, the hole concentration continues to decrease with time (not shown here) but with reaction rates significantly differing from GaH pair formation shown in Figure 1a. It is therefore likely that this effect is not GaH pair associated, but may have to do with thermal donors.[15] For this reason, it is not possible to state whether GaH pair dissociation occurs in the

dark for prolonged annealing as it does for BH pairs,[11,15,16] but it does not occur on the timescales of this study, in accordance to other investigations.[16]

The situation changes tremendously, if an injection of $\Delta n = 1.4 \times 10^{16}\,\text{cm}^{-3}$ is applied (Figure 1b). The behavior now can be described by the sum of two exponential decays with differing effective reaction rates $R_{1,2}$ and amplitudes $A_{1,2}$ to account for the two time-shifted decays

$$-\Delta p(t) = A_1 \times \exp(-R_1 \times t) + A_2 \times \exp(-R_2 \times t) + A_\infty \qquad (4)$$

A subsequent dark anneal ($T = 180\,°C$) does not change pair concentration significantly, as depicted in Figure 1c, although there might be a small change in hole concentration possibly attributed to the aforementioned formation of thermal donors.

During illumination, both dissociation dynamics occur with such a time lag that a plateau appears to form (indicated by II in Figure 1b). To investigate the properties of the plateau (state II), another sample again was annealed in the dark to trigger GaH pair formation, as depicted in **Figure 2**a. The scale of $-\Delta p$ was arbitrarily shifted to the minimum value of the pair concentration, which is why the scaling is different from that in Figure 1. The subsequent light soaking was interrupted after 10^4 s (state II,
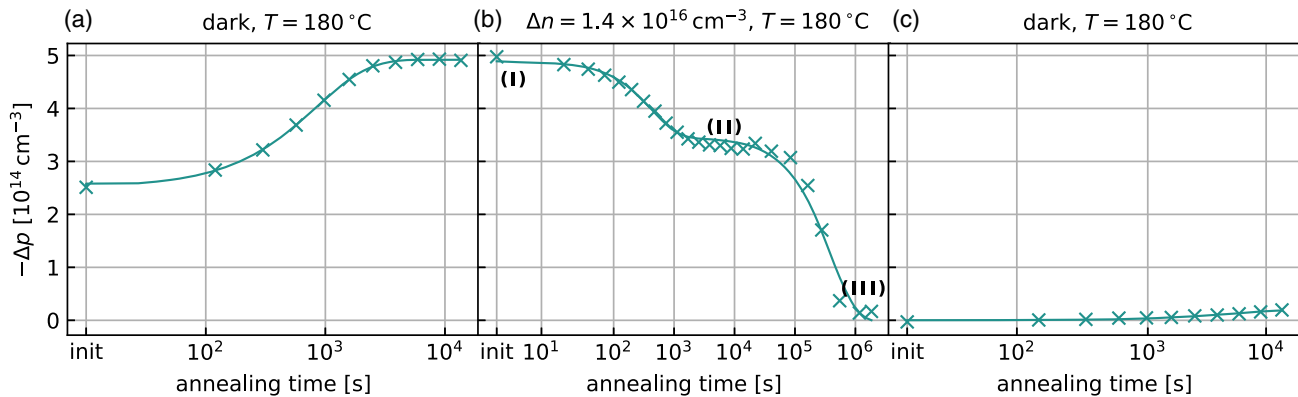

Figure 1. Change in charge carrier concentration $-\Delta p$ as a measure for change in pair concentration: $\Delta[\text{GaH}] = -\Delta p$. a) Formation of GaH pairs upon dark anneal, fit according to Equation (3). b) Dissociation of GaH pairs at a constant injection level $\Delta n = 1.4 \times 10^{16}\,\text{cm}^{-3}$, fit according to Equation (4). c) Change in hole concentration after subsequent dark anneal indicates no significant reformation of GaH pairs.
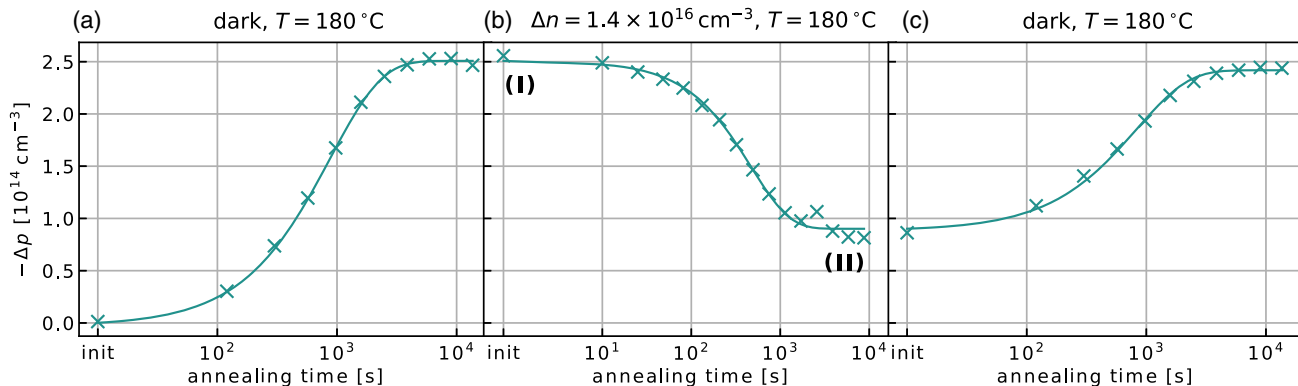

Figure 2. Change in charge carrier concentration $-\Delta p$ as a measure for change in pair concentration: $\Delta[\text{GaH}] = -\Delta p$. a) Formation of GaH pairs upon dark anneal, fit according to Equation (3). b) Partial dissociation of GaH pairs at a constant injection level $\Delta n = 1.4 \times 10^{16}\,\text{cm}^{-3}$, fit according to Equation (4) with $R_2 \to \infty$. c) GaH pairs reform during subsequent dark annealing.

see Figure 2b) and the sample was placed in the dark at 180 °C. As depicted in Figure 2c, the dark anneal triggers the formation of GaH pairs again. This behavior can be observed in the case of BH pairs as well.[13] This leads to the conclusion that there are two processes ongoing, a fast, reversible one and a much slower, irreversible dissociation of gallium–hydrogen pairs in crystalline silicon. The design of our experiment does not allow us to distinguish whether these are two independent processes or a cascade reaction takes place. We assume the fast, reversible dissociation to be a shift of the reaction (Equation (2)) from the pairs towards unpaired H/H_{2A} and Ga, whereas the second drop in pair concentration may be due to the transition of hydrogen into a different, more stable configuration or effusion. To get further insight into the process of dissociation, the following sections will describe the injection and temperature dependence of the dissociation.

2.1. Injection Dependence of Dissociation

As shown in **Figure 3**, the fraction and rate of dissociation of GaH pairs after they have been formed at 180 °C in the dark can be tuned by changing the injection level. It should be noted that the scaling of the ordinate differs compared with the other figures, since the initial values were used as reference state. Therefore, a decrease in [GaH] leads to negative values of $-\Delta p$. This makes it easier to see trends in dissociation rates and amplitudes. In general, a higher injection level leads to a faster reaction but also a more pronounced decrease in pair concentration. This is expressed in the fact that the level of state II decreases with increasing injection. The increment of injection leads to a decrease of the level of state II of around $3 \times 10^{14} \, \text{cm}^{-3}$ upon raising applied injection from 1.4×10^{15} to $3.7 \times 10^{16} \, \text{cm}^{-3}$. However, exact quantitative comparisons are difficult since we cannot exclude some temperature fluctuations in the applied firing process that might lead to differing total hydrogen content between the samples.[5,22] Since we assume first order kinetics, that is, the dissociation rate is proportional to the pair concentration, differing initial pair concentrations should not influence the analysis of dissociation rate constants R_1.

The reaction rate R_1 for the first, reversible dissociation of GaH pairs as a function of injection is depicted in **Figure 4**.
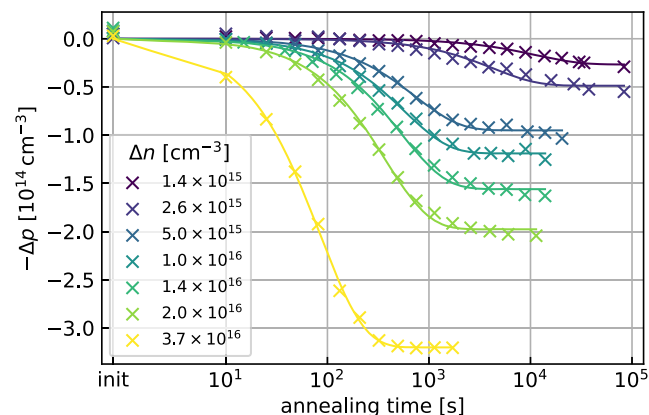
Figure 3. Change in gallium–hydrogen pair concentration at several injection levels at 180 °C measured by negative change in hole concentration $-\Delta p$. Lines are fits according to Equation (4) with $R_2 \to \infty$.
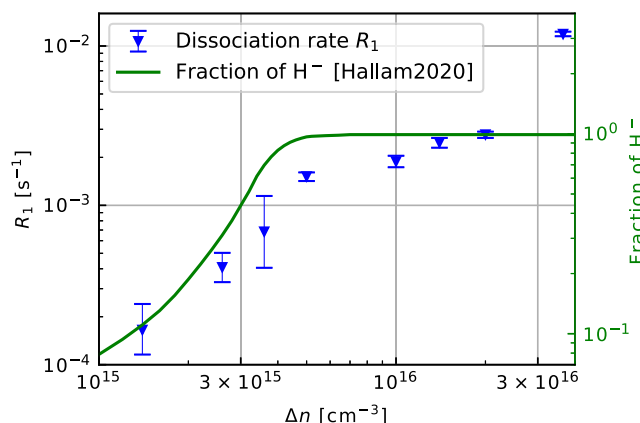
Figure 4. Reaction rate R_1 of the dissociation of gallium–hydrogen pairs as a function of injection Δn obtained by fitting Equation (4) to the change in hole concentration. Error bars mark the interval of R_1 at which the RMS error does not exceed its minimum by more than 5%.

The shown uncertainties are determined by the range of R_1 which leads to a root-mean-square (RMS) error not greater than 5% above its minimum.

Interestingly, the rate R_1 shows a strong increase with injection up to an injection level of $5 \times 10^{15} \, \text{cm}^{-3}$, but a much less pronounced injection dependence between 5×10^{15} and $2 \times 10^{16} \, \text{cm}^{-3}$. Above this range, the rate of dissociation seems to increase strongly again. Since the absolute concentration of pairs dissociating at lower injection levels drops, the uncertainty increases strongly. Furthermore, an influence of thermal donors on rate determination cannot be excluded, which becomes relevant only for long treatment times applied during the low injection levels.

The dissociation of GaH pairs requires that neutral dimers H_2 form from positively charged hydrogen atoms. The reaction $H^+ + H^+ \to H_2 + 2h^+$ seems less likely than $H^- + H^+ \to H_2$ due to the repulsive Coulomb interaction. For this reason, we expect the reaction probability to scale with the fraction of H^-. This fraction depends on the Fermi level,[23,24] which in turn depends on temperature and excess charge carriers. The fraction of negatively charged hydrogen H^- on total hydrogen concentration is plotted on the same graph with the dissociation rate constant. The data are taken from the study by Hallam et al.[24] based on the method by Sun et al.[23] As shown, the fraction of H^- increases more for low injections than with higher injections and resembles the behavior of the dissociation rate R_1.

For low injections, the fraction of H^- is low, such that the formation of neutral dimers H_2 is not favored. If the injection is increased, the fraction of negatively charged hydrogen increases as well, such that the formation of neutral dimers H_2 is more likely. We therefore conclude that the speed of reaction for the dissociation of GaH pairs is determined by the fraction of negatively charged hydrogen H^-. However, the renewed sharp increase in the reaction rate at $3.2 \times 10^{16} \, \text{cm}^{-3}$ cannot be explained on the basis of the present data.

2.2. Temperature Dependence of Dissociation

In addition to the determination of the injection dependence, the experimental procedure also allows the determination of the
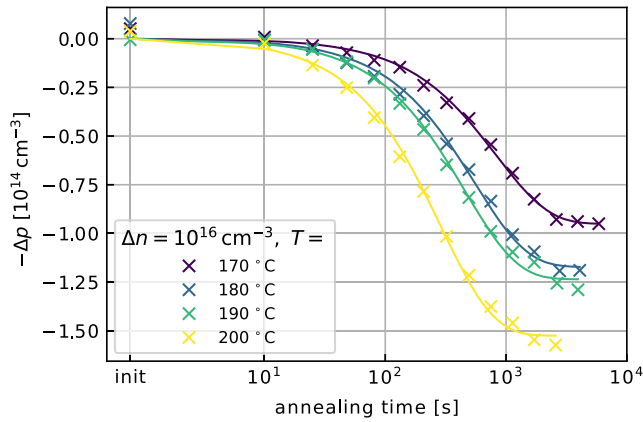
Figure 5. Change in gallium–hydrogen pair concentration at several temperatures and an injection level of $\Delta n = 1 \times 10^{16}\,\text{cm}^{-3}$ measured by change in hole concentration $-\Delta p$.

activation energy of dissociation under illumination. For this purpose, the reaction rate R_1 of the dissociation from state I to state II (Equation (4)) at different temperatures but constant injection levels of 5×10^{15} and $1 \times 10^{16}\,\text{cm}^{-3}$ was determined analogously as in Section 2.1. The level of state II decreases around $5 \times 10^{13}\,\text{cm}^{-3}$ upon raising annealing temperature from 170 to 200 °C, as shown in **Figure 5**. A similar behavior can be observed for an injection level of $\Delta n = 5 \times 10^{15}\,\text{cm}^{-3}$ (not shown).

The respective rate R_1 of dissociation is plotted against inverse temperature in **Figure 6**. As shown in the graph, the dissociation rates follow Arrhenius' equation

$$R(T) = R_0 \times \exp\left(-\frac{E_A}{k_B T}\right) \qquad (5)$$

with Boltzmann's constant k_B, the temperature-independent trial frequency R_0, and the activation energy E_A. This allows for the determination of the activation energies $E_A^{5e15} = 0.71(5)\,\text{eV}$ ($\Delta n = 5 \times 10^{15}\,\text{cm}^{-3}$) and $E_A^{1e16} = 0.64(7)\,\text{eV}$ ($\Delta n = 1 \times 10^{16}\,\text{cm}^{-3}$).
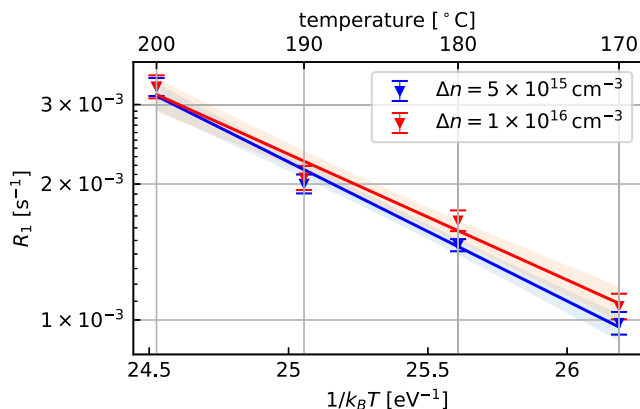

Figure 6. Effective reaction rate R_1 of the dissociation of gallium–hydrogen pairs as a function of inverse temperature $1/k_B T$ for the injection levels $\Delta n = 5 \times 10^{15}\,\text{cm}^{-3}$ and $\Delta n = 1 \times 10^{16}\,\text{cm}^{-3}$. Lines are fits to the Arrhenius Equation (5) with a 68% uncertainty interval.

Although the determined activation energies are compatible within the limits of their uncertainty, there might be a trend toward a lower activation energy with increasing injection which could be caused by the additional charge carriers present.

2.3. Impact on Lifetime

The change in lifetime-equivalent defect density $\Delta N_{\text{leq}} = \tau_{\text{eff}}^{-1} - \tau_{\text{eff,ref}}^{-1}$ with respect to $t_{\text{ref}} = 15\,\text{s}$ during illuminated annealing can provide injection-dependent information on whether and what kind of recombination-active defects form. This is complemented by the analysis of the surface recombination parameter J_0. The corresponding data during the illuminated anneal (state I to state III) are shown in **Figure 7**. A slight decrease in surface defect density in the beginning, visible in the specific color sequence of ΔN_{leq} and in J_0, occurs in a time frame where the decay of GaH is not yet pronounced. The reversible dissociation of GaH pairs (state I to II) up to $10^4\,\text{s}$ does not affect ΔN_{leq} too much, although there might be an increase in recombination active centers in the bulk around $10^2\,\text{s}$. For longer treatment times around $10^5\,\text{s}$ there is a strong increase in ΔN_{leq}, coinciding with the second drop in pair concentration. The analysis of J_0 and the specific color sequence of ΔN_{leq} suggests a formation of defects at the surface around $10^5\,\text{s}$. For even longer times, the color sequence of ΔN_{leq} inverts suggesting the formation of bulk defects. It is unclear whether the apparent drop in J_0 is at least in parts an artifact due to this bulk defect formation.
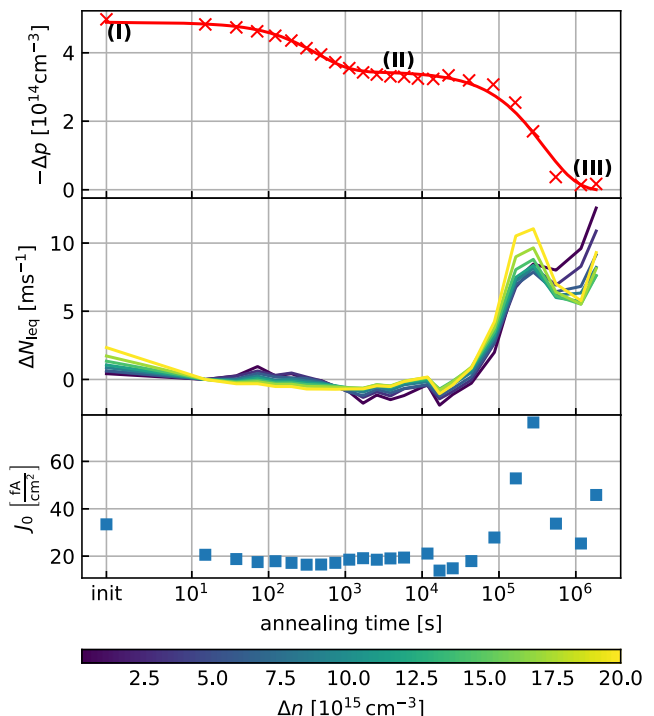

Figure 7. Change in $-\Delta p = \Delta[\text{GaH}]$ in comparison with the change in lifetime-equivalent defect density ΔN_{leq} and surface recombination parameter J_0 during illuminated annealing at 180 °C.

ADVANCED SCIENCE NEWS
www.advancedsciencenews.com

pss rrl
physica status solidi
www.pss-rapid.com

Especially the long-term behavior leaves room for speculations about a possible common mode of action of irreversible GaH pair dissociation in the bulk and formation of defects at the surface—maybe the effusion of hydrogen from the bulk (at first only draining the reservoir for reversible GaH pair formation, but later even leading to re-activation of H-passivated bulk defects) and its accumulation at or underneath the surface. On the other hand, the increase in surface defect density might suggest a loss of hydrogen from otherwise H-terminated dangling bonds and thus rather a depletion at the surface caused by insufficient supply of hydrogen from the bulk drained more by effusion. However, the presented data do not allow for detailed conclusions.

3. Conclusion

After fast firing of silicon wafers with deposited hydrogen-rich dielectric layers (SiN$_x$:H), the introduced hydrogen forms gallium–hydrogen pairs upon annealing at elevated temperatures in the dark.

If illumination is applied, two phases of dissociation can be observed. First, a relatively fast, reversible but only partial dissociation takes place. The strong dependence on temperature and injection suggests an electron-driven, thermally activated back reaction into either hydrogen dimers and/or atomic hydrogen. The activation energies $E_A^{\Delta n}$ for two injection levels Δn could be determined to be $E_A^{5e15} = 0.71(5)\,\text{eV}$ and $E_A^{1e16} = 0.64(7)\,\text{eV}$ for $\Delta n = 5 \times 10^{15}$ and $1 \times 10^{16}\,\text{cm}^{-3}$, respectively. A second decay in pair concentration occurs later and is irreversible in a sense that GaH pairs do not form again in the dark after this treatment. Furthermore, this second drop is temporally correlated with an increase in defect density, which can be partially attributed to degradation of surface passivation quality.

4. Experimental Section

Sample Preparation: During sample preparation, commercially available gallium-doped monocrystalline Czochralski-grown wafers (1 Ω cm, Longi) were saw damage etched (KOH, 8 min at 80 °C) and cleaned (surface oxidation by ozone and subsequent HF dip). SiN$_x$:H layers were deposited on both sides with a thickness of 100 nm in a plasma-enhanced chemical vapor deposition process (reactive gases: SiH$_4$:NH$_3$ = 27:13; carrier gas: N$_2$; temperature 400 °C, duration per side: 120 s; PlasmaLab 100, Oxford Instruments).

The nonmetallized samples were fired in a belt furnace with a measured sample peak temperature of 850(10) °C to provide H-rich samples and cut into 5 × 5 cm^2 samples. The process flow used here aimed to maximize the hydrogen input into the Si bulk, ignoring the influence on (initial) lifetime of the excess charge carriers. Stripe-shaped contacts were produced by thermal evaporation of aluminum and subsequent laser pulses to form laser-fired contacts (LFCs),[25] allowing for direct contact resistivity measurements (as described in the study by Herguth et al.[14]) to quantify the change in hole concentration and thus change in the amount of GaH pairs in the bulk.

Samples were annealed on a hot plate that was either covered (dark) or illuminated by a homogenized laser system ($\lambda = 808\,\text{nm}$) with adjustable photon flux. Photon flux was determined by the analysis of short-circuit current of a calibrated reference cell, as suggested by Herguth.[26]

For the determination of excess charge carrier lifetime, a temperature-controlled Sinton Instruments WCT-120TS lifetime tester in quasi-steady-state condition was used. The data measured at annealing temperature were used to calculate the required photon flux to maintain a constant injection level during annealing.

Resistivity Measurements: Resistivity measurements were performed with a digital multimeter (Keithley 2000, 6.5-digit) on a temperature-stabilized measurement setup, as established by Herguth and Winter.[14] The (negative) change in hole concentration $-\Delta p = p_0 - p$ with respect to a reference state (p_0, R_0) was calculated from the resistance R by

$$-\Delta p = \frac{d \times g}{q \times w \times t}\left(\frac{1}{\mu_{p,0}R_0} - \frac{1}{\mu_p R}\right) \tag{6}$$

with the dimensions t as thickness, w as width, d as distance of the Al contacts of the sample, and a geometry factor $g = 1.02$ to account for inhomogeneous current flow. Hole mobilities for the respective temperature and hole concentration were taken from the PVLighthouse mobility calculator.[27] Assuming that p was given by the net doping potentially impacted by GaH pairs, thus $p = N_{\text{dop}} - [\text{GaH}]$, then an increase in pair density $\Delta[\text{GaH}]$ corresponded to a decrease in hole density Δp; thus, $\Delta[\text{GaH}] = -\Delta p$.

Analysis of Lifetime Dynamics: Injection-dependent lifetime data were further analyzed with regard to possible formation of recombination active defects at the surface or in the bulk during annealing under illumination.

Surface recombination was quantified in terms of the recombination parameter J_0[28] indicating that excess carrier lifetime has a characteristic dependence on injection Δn: $\tau_{\text{surf}}^{-1} \propto (p_0 + \Delta n) \times J_0$. Analysis took place at an injection of $2 \times 10^{16}\,\text{cm}^{-3}$ using the method of Kimmerle et al.[29] It should be noted that this method relies on the slope with injection and is susceptible to other bulk-related lifetime components that impact that slope. This is significant in the case shown insofar as that the analysis took place at an injection resembling the doping level ($1.5 \times 10^{16}\,\text{cm}^{-3}$) where (emerging) bulk defects may lead to a systematic underestimation of J_0. In this sense, the shown J_0 values were to be understood as lower limits, in particular when bulk defects were numerous.

Furthermore, defect dynamics in general were analyzed in terms of a lifetime-equivalent defect density ΔN_{leq}[30] changing with time according to $\Delta N_{\text{leq}} = \tau_{\text{eff}}^{-1} - \tau_{\text{eff,ref}}^{-1}$ calculated with respect to a reference time from the injection-dependent effective lifetime τ_{eff}. Note that ΔN_{leq} was designed to cancel out lifetime components that did not change and that the specific injection dependence of ΔN_{leq} could be used to conclude what kind of defect was formed. In particular, the emergence of defects at the surface expressed by an increase of J_0 implied a stronger increase in ΔN_{leq} at higher than at lower injection levels. In contrast, the emergence of bulk defects with energy levels deep in the bandgap implied a more pronounced increase in ΔN_{leq} at lower than at higher injection levels.[30]

Conflict of Interest

The authors declare no conflict of interest.

Data Availability Statement

The data that support the findings of this study are available from the corresponding author upon reasonable request.

[1] M. A. Jensen, A. Zuschlag, S. Wieghold, D. Skorka, A. E. Morishige, G. Hahn, T. Buonassisi, *J. Appl. Phys.* **2018**, *124*, 085701.

[2] T. H. Fung, M. Kim, D. Chen, C. E. Chan, B. J. Hallam, R. Chen, D. N. Payne, A. Ciesla, S. R. Wenham, M. D. Abbott, *Sol. Energy Mater. Sol. Cells* **2018**, *184*, 48.

[3] J. Schmidt, D. Bredemeier, D. C. Walter, *IEEE J. Photovoltaics* **2019**, *9*, 1497.

[4] D. Chen, P. Hamer, M. Kim, C. Chan, A. Ciesla nee Wenham, F. Rougieux, Y. Zhang, M. Abbott, B. Hallam, *Sol. Energy Mater. Sol. Cells* **2020**, *207*, 110353.

[5] S. Jafari, U. Varshney, B. Hoex, S. Meyer, D. Lausch, *IEEE J. Photovoltaics* **2021**, *11*, 1363.

[6] J. I. Pankove, D. E. Carlson, J. E. Berkeyheiser, R. O. Wance, *Phys. Rev. Lett.* **1983**, *51*, 2224.

[7] C. Sah, J. Y. Sun, J. J. Tzou, *Appl. Phys. Lett.* **1983**, *43*, 204.

[8] J. I. Pankove, P. J. Zanzucchi, C. W. Magee, G. Lucovsky, *Appl. Phys. Lett.* **1985**, *46*, 421.

[9] M. Stavola, S. J. Pearton, J. Lopata, W. C. Dautremont-Smith, *Appl. Phys. Lett.* **1987**, *50*, 1086.

[10] M. Stavola, S. J. Pearton, J. Lopata, W. C. Dautremont-Smith, *Phys. Rev. B* **1988**, *37*, 8313.

[11] V. V. Voronkov, R. Falster, *Phys. Status Solidi B* **2017**, *254*, 1600779.

[12] D. C. Walter, D. Bredemeier, R. Falster, V. V. Voronkov, J. Schmidt, *Sol. Energy Mater. Sol. Cells* **2019**, *200*, 109970.

[13] (Eds: D. C. Walter, D. Bredemeier, R. Falster, V. V. Voronkov, J. Schmidt), In *Proc. of the 37th European Photovoltaic Solar Energy Conf. and Exhibition*, WIP, Munich **2020**, pp. 140–144.

[14] A. Herguth, C. Winter, *IEEE J. Photovoltaics* **2021**, *11*, 1059.

[15] C. Winter, J. Simon, A. Herguth, *Phys. Status Solidi A* **2021**, *218*, 2100220.

[16] Y. Acker, J. Simon, A. Herguth, *Phys. Status Solidi A* **2022**, *219*, 2200142.

[17] D. C. Walter, V. V. Voronkov, R. Falster, D. Bredemeier, J. Schmidt, *J. Appl. Phys.* **2022**, *131*, 165702.

[18] P. M. Weiser, E. Monakhov, H. Haug, M. S. Wiig, R. Søndenå, *J. Appl. Phys.* **2020**, *127*, 065703.

[19] J. Simon, A. Herguth, G. Hahn, *J. Appl. Phys.* **2022**, *131*, 235703.

[20] M. J. Binns, S. A. McQuaid, R. C. Newman, E. C. Lightowlers, *Semicond. Sci. Technol.* **1993**, *8*, 1908.

[21] R. E. Pritchard, J. H. Tucker, R. C. Newman, E. C. Lightowlers, *Semicond. Sci. Technol.* **1999**, *14*, 77.

[22] S. Wilking, S. Ebert, A. Herguth, G. Hahn, *J. Appl. Phys.* **2013**, *114*, 194512.

[23] C. Sun, F. E. Rougieux, D. Macdonald, *J. Appl. Phys.* **2015**, *117*, 045702.

[24] B. J. Hallam, P. G. Hamer, A. M. Ciesla née Wenham, C. E. Chan, B. Vicari Stefani, S. Wenham, *Prog. Photovoltaics: Res. Appl.* **2020**, *28*, 1217.

[25] E. Schneiderlöchner, R. Preu, R. Lüdemann, S. W. Glunz, *Prog. Photovoltaics: Res. Appl.* **2002**, *10*, 29.

[26] A. Herguth, *Energy Procedia* **2017**, *124*, 53.

[27] PV Lighthouse, Mobility Calculator. https://www2.pvlighthouse.com.au/calculators/mobility%20calculator/mobility%20calculator.aspx (accessed: April 2020).

[28] K. R. McIntosh, L. E. Black, *J. Appl. Phys.* **2014**, *116*, 014503.

[29] A. Kimmerle, J. Greulich, A. Wolf, *Sol. Energy Mater. Sol. Cells* **2015**, *142*, 116.

[30] A. Herguth, *IEEE J. Photovoltaics* **2019**, *9*, 1182.